J. Plasma Phys. (2023), *vol*. 89, 965890502
Published by Cambridge University Press

doi:10.1017/S0022377823001162

Beam current from downramp injection in electron-driven plasma wakefields

Céline Hue [1], Anton Golovanov [1,†], Sheroy Tata [1], Sébastien Corde [2] and Victor Malka [1]

[1]Department of Physics of Complex Systems, Weizmann Institute of Science, 7610001 Rehovot, Israel

[2]LOA, ENSTA Paris, CNRS, Ecole Polytechnique, Institut Polytechnique de Paris, 91762 Palaiseau, France

(Received 28 June 2023; revised 10 October 2023; accepted 11 October 2023)

We study the stability of plasma wake wave and the properties of density-downramp injection in an electron-driven plasma accelerator. In this accelerator type, a short high-current electron bunch (generated by a conventional accelerator or a laser–wakefield acceleration stage) drives a strongly nonlinear plasma wake wave (blowout), and accelerated electrons are injected into it using a sharp density transition which leads to the elongation of the wake. The accelerating structure remains highly stable until the moment some electrons of the driver reach almost zero energy, which corresponds to the best interaction length for optimal driver-to-plasma energy transfer efficiency. For a particular driver, this efficiency can be optimised by choosing appropriate plasma density. Studying the dependence of the current of the injected bunch on driver and plasma parameters, we show that it does not depend on the density downramp length as long as the condition for trapping is satisfied. Most importantly, we find that the current of the injected bunch primarily depends on just one parameter which combines both the properties of the driver (its current and duration) and the plasma density.

Key words: intense particle beams, plasma waves, plasma simulation

1. Introduction

Plasma accelerators that rely on high-amplitude plasma wakefields are promising several orders of magnitude higher acceleration gradients than in conventional radio-frequency accelerators (Malka *et al.* 2008; Esarey, Schroeder & Leemans 2009). The two main types of plasma accelerators are laser–wakefield accelerators (LWFAs) based on driving a plasma wake with a short intense laser pulse (Tajima & Dawson 1979) and plasma–wakefield accelerators (PWFAs) based on using a short high-current particle bunch as a driver (Chen *et al.* 1985; Rosenzweig *et al.* 1991). LWFAs have demonstrated rapid growth both in terms of the energy of accelerated electrons (reaching energies of 8 GeV at a distance of 20 cm Gonsalves *et al.* 2019) and stability of beam properties

† Email address for correspondence: anton.golovanov@weizmann.ac.il

(Faure *et al.* 2006). For PWFA, experimental studies have demonstrated high-gradient acceleration (Blumenfeld *et al.* 2007) and efficient energy transfer from the driver to the witness (Litos *et al.* 2014; Lindstrøm *et al.* 2021).

Despite some advantages such as the long dephasing length and a more stable wakefield structure, PWFAs saw comparatively less development than LWFAs because the sources of short (comparable to plasma wavelength) electron bunches with a high enough current to excite a nonlinear wake were not widely available. Recently, the concept of hybrid LWFA–PWFA multistaged plasma accelerators (Hidding *et al.* 2010; Kurz *et al.* 2021; Foerster *et al.* 2022) based on the idea of using electron bunches from the first LWFA stage to drive a second PWFA stage has started gaining popularity, broadening the possibilities for experimental PWFA studies. LWFA-produced electron bunches are very short and high current, so they naturally have excellent parameters to drive a highly nonlinear (blowout) plasma wake. The density-downramp injection technique also proved to be an effective way of injecting electrons in the PWFA stage (Grebenyuk *et al.* 2014; Martinez de la Ossa *et al.* 2017; Xu *et al.* 2017; Zhang *et al.* 2019; Couperus Cabadağ *et al.* 2021). Even though the electron-driven second stage cannot significantly surpass the performance of the first LWFA stage in terms of the total energy of the accelerated electrons, due to its stable nature it can serve as a 'quality booster' by generating bunches with improved properties (Martinez de la Ossa *et al.* 2017; Foerster *et al.* 2022). However, although relatively high energy transfer efficiency is achieved and high-quality beams with hundreds of megaelectronvolts are predicted, the energy stability for such accelerator in previous research is still comparable to the single-stage LWFAs (Foerster *et al.* 2022), and more studies are required to understand the parameter dependence and physics behind this stage.

For PWFA to be efficient, one of the important steps is to optimise the driver-to-witness energy transfer efficiency. The beam currents of both the driver and the witness beams play decisive roles in optimising the energy transfer efficiency. Few studies so far have systematically focused on controlling the beam currents produced in plasma-based accelerators. The production in LWFA of the current profile finely tuned for the use in the second stage was studied in Hue *et al.* (2023), but studies for PWFAs are lacking.

In this paper, we focus on the performance of a PWFA based on density-downramp injection of electrons. One important step in calculating and optimising the energy transfer efficiency is to understand the beam dynamics. Previous research described such important phenomena as the hosing instability experienced at the tail of the bunch (Huang *et al.* 2007), beam head erosion (Zhou *et al.* 2007; Li *et al.* 2012; An *et al.* 2013), energy depletion (Muggli *et al.* 2010) and the transformer ratio (Blumenfeld *et al.* 2010). Yet, driver parameters used in these studies corresponded mostly to electron beams produced by conventional linear accelerators, which are very different from beams produced in LWFA stage for hybrid accelerators. In this article, the dynamics of flattop–current electron drivers with a total beam charge of 100–500 pC, 100–300 MeV energy typical for the LWFA-produced bunches (Hue *et al.* 2023) is studied. In § 2, the stability of the wakefield and driver-to-plasma energy transfer efficiency are discussed. In § 3, we numerically study density-downramp injection in the PWFA stage and the dependence of the current of the injected electron bunch on the parameters of the driver, the plasma and the downramp. Despite having such a multidimensional parameter space, we demonstrate that the injected current is determined mostly by one parameter, the effective current $J_{\text{eff}} = J_b(k_p\xi_b)^{2/3}$, which combines both the properties of the driver (its current J_b and length ξ_b) and the plasma (wavenumber k_p). The dependence of the witness current on this parameter is linear. We also show the limitation of this scaling for longer driver bunches which cannot efficiently excite a nonlinear wake.

https://doi.org/10.1017/S0022377823001162 Published online by Cambridge University Press

2. Driver stability and driver-to-plasma efficiency

In this section, we study the evolution and propagation of an electron beam in PWFA assuming fully preionised plasma. For sufficiently short, tightly focused and high-current beams, the wakefield is excited in the strongly nonlinear ('bubble' or 'blowout') regime (Rosenzweig *et al.* 1991; Pukhov & Meyer-ter-Vehn 2002; Lotov 2004), when a cavity (a bubble) devoid of plasma electrons is formed behind the driver. The excitation of the bubble by an electron beam can be self-consistently described by a model by Golovanov *et al.* (2021) which can be used to calculate the shape of the bubble as well as the distribution of all the fields in it based solely on the charge density distribution of the driver. As this model is based on the relativistic limit of the theory by Lu *et al.* (2006), it is strictly valid only in the case when the transverse size of the bubble R_{bub} is large in terms of plasma units, $k_p R_{\mathrm{bub}} \gg 1$, which is not necessarily the case for the parameters considered in the paper. A more accurate model for comparatively small bubbles ($k_p R_{\mathrm{bub}} \sim 1$) was recently proposed in Golovanov *et al.* (2023), but it lacks simple analytical scalings. Theoretical models also cannot fully describe the driver evolution and self-injection, and thus cannot completely replace numerical simulations. Still, we can use the predictions of the models to compare with the simulation results.

To study the evolution of the driver in PWFA, we perform numerical simulations of the beam–plasma interaction using the 3D quasistatic particle-in-cell (PIC) code QuickPIC (Huang *et al.* 2006). The beam has the mean energy of 250 MeV and the charge of 137 pC (corresponding to the total energy of 17 mJ) with a flattop longitudinal current profile with the length $\xi_b = 13.4\,\mu\mathrm{m}$ (or the duration 45 fs corresponding to the current of 3.1 kA) and a Gaussian transverse profile $\exp(-r^2/2\sigma_r^2)$ with radius $\sigma_r = 0.52\,\mu\mathrm{m}$ and normalised emittance of $\epsilon_{x,y} = 0.42\,\pi\mathrm{mm\,mrad}$ defined as $\epsilon_x = (mc)^{-1}\sqrt{\langle x^2\rangle\langle p_x^2\rangle - \langle xp_x\rangle^2}$. The peak number density of the beam $n_b = 3.75 \times 10^{19}\,\mathrm{cm}^{-3}$. The chosen parameters correspond to typical electron beams generated by the density-downramp injection in the first LWFA stage and are taken from simulations in Hue *et al.* (2023). In fact, as will be briefly explained in the next section, the tunability of the LWFA-produced driver parameters is fairly limited.

The plasma density n_0 is chosen to be much lower than the density of the beam n_b, so that the driver excites a highly nonlinear plasma wakefield or a bubble (see figure 1). In the simulation, we use a box with the size of $6k_p^{-1} \times 6k_p^{-1} \times 7k_p^{-1}$ and $512 \times 512 \times 256$ cells (the beam propagates along z), where $k_p = \omega_p/c$ is the plasma wavenumber corresponding to the plasma density n_0, $\omega_p = (n_0 e^2/m\varepsilon_0)^{1/2}$ and ε_0 is the vacuum permittivity. The number of particles per cell for the background plasma is 4, and for the beam the total number of macroparticles is 2^{21}. The simulation timestep is equal to $5\omega_p^{-1}$.

The transverse emittance of the beam is chosen to be close to matched to the plasma density to prevent significant changes of the transverse size (the matched plasma density for the chosen beam parameters is $2.74 \times 10^{17}\,\mathrm{cm}^{-3}$). In this wakefield, the driver generally experiences two forces: the focusing force from the ion column (linear in the distance r from the axis inside the bubble and leading to betatron oscillations of the electrons of the driver) and the decelerating longitudinal force. We observe that the accelerating structure remains highly stable before rapidly collapsing when electrons of the driver start dephasing due to deceleration to very low energies. This inherent stability owes to the fact that the changing transverse distribution of the almost matched driver does not influence the structure of the bubble, whereas the longitudinal velocity of the ultrarelativistic particles of the bunch stays almost equal to the speed of light until some of the electrons are decelerated to subrelativistic energies, corresponding to the moment of collapse (compare

https://doi.org/10.1017/S0022377823001162 Published online by Cambridge University Press

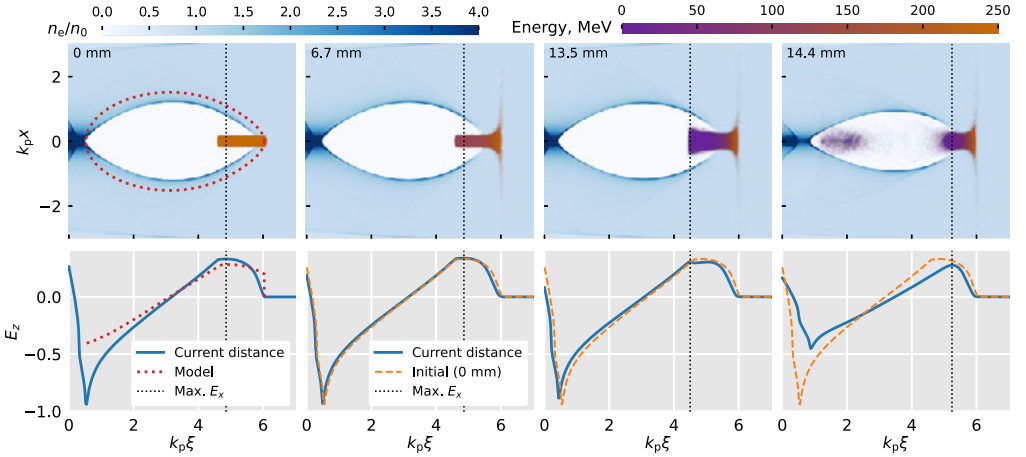

FIGURE 1. Electron density n_e distributions and the longitudinal electric fields E_z on the axis in a wake driven by an electron driver at different propagation distances. The dashed lines show the initial distribution of the accelerating field at 0 mm. For the driver, the colour shows the energy of particles. The dotted lines at 0 mm show the analytical solution according to the model in Golovanov *et al.* (2023). Vertical dotted lines show the position of the maximum decelerating field E_z. Plasma density $n_0 = 3.125 \times 10^{17}\ \mathrm{cm}^{-3}$.

the first three distances in figure 1 before the collapse to the fourth after the collapse began).

The propagation length corresponding to this collapse is much shorter than the distance of particle loss due to head erosion or beam hosing instability, so it effectively determines the PWFA stage length. Head erosion usually happens due to the initial emittance of the driver in the region at the head of the bunch where the gas is not yet ionised by its fields and, thus, the head propagates effectively in vacuum and experiences no focusing from the plasma (Zhou *et al.* 2007; Li *et al.* 2012; An *et al.* 2013). The Coulomb self-force is proportional to γ^{-2} and can be usually ignored for ultrarelativistic bunches. When the plasma is preionised, head erosion can still happen because the wakefield providing the focusing force is not yet strong enough at the head of the bunch, but its effect is much smaller than in the initially neutral gas (An *et al.* 2013). As the head erodes, it still continues to drive a lower-amplitude wake behind it, which makes the spread of this erosion to other parts of the bunch very slow. As can be seen from figure 1, it leads only to a small shift in the phase of the nonlinear wake over the propagation distance and cannot significantly affect the acceleration process.

Another effect which is believed to limit the length of PWFAs is the hosing instability which should lead to the exponential growth in oscillations of the beam centroid and the corresponding growth of oscillations of the bubble (Huang *et al.* 2007). However, recent research suggests that energy depletion of the driver as well as its energy spread or energy chirp can efficiently suppress and saturate this instability due to the dephasing of betatron oscillations (Mehrling *et al.* 2017, 2019). In our simulations, hosing is not taken into account as the initial charge density distribution is ideally symmetric.

Thus, energy depletion of the driver is the main mechanism which determines the acceleration length. It leads to electrons reaching subrelativistic energies, after which significant portion of the electrons of the driver are quickly lost and the accelerating structure collapses (see figure 1 at 14.4 mm). For a bunch with no energy chirp, this process

https://doi.org/10.1017/S0022377823001162 Published online by Cambridge University Press

			L_{col} (mm)		η, %	
n_0 (cm^{-3})	n_b/n_0	$k_p\xi_b$	Simulation	Model	Simulation	Model
2.5×10^{18}	15	3.99	4.8	6.0	65	73
1.875×10^{18}	20	3.45	5.5	7.1	71	81
1.25×10^{18}	30	2.82	6.7	8.1	76	87
6.25×10^{17}	60	1.99	9.4	11.6	77	93
4.17×10^{17}	90	1.63	11.6	14.1	75	93
3.125×10^{17}	120	1.41	13.5	16.4	73	92

TABLE 1. The collapse length of the electron driver L_{col} observed in quasistatic PIC simulations and estimated from (2.1) as well as the efficiency η calculated according to (2.2) and estimated based on the model from Golovanov *et al.* (2023) for different plasma densities n_0.

happens at the point of the peak decelerating electric field the value of which can be estimated from the solution based on the model in Golovanov *et al.* (2023) (shown with dotted lines in figure 1 at 0 mm). The length at which the accelerating structure collapse happens can, thus, be estimated as the length at which an electron with the kinetic energy $K \approx \gamma mc^2$ is decelerated to zero energy in the field $E_{\max}$,

$$L_{\text{col}} \approx \frac{\gamma mc^2}{eE_{\max}}, \tag{2.1}$$

where γ is the Lorentz factor, m is the electron mass, $e > 0$ is the elementary charge and c is the speed of light. The comparison to values observed in the simulations (see table 1) provides a fairly good estimate for the collapse length.

When the collapse of the accelerating structure begins, the driver still has part of its energy left (as decelerating field is non-uniform, and different parts of the driver experience different field values), which limits driver-to-plasma energy transfer efficiency defined as the percentage of the bunch initial energy spent on generating the wakefield by the moment the collapse begins,

$$\eta = \frac{\langle\gamma\rangle_0 - \langle\gamma\rangle_{\text{col}}}{\langle\gamma\rangle_0}, \tag{2.2}$$

where averaging is performed over the bunch particles. Assuming that the bunch is monoenergetic, it can also be estimated as $\eta \approx \langle E_z\rangle / E_{\max}$, so the efficiency mostly reflects how uniform the distribution of the decelerating electric field inside the driver is. The comparison between the actual efficiency observed in simulations to the estimated efficiency based on the field distribution E_z according to the model by Golovanov *et al.* (2023) is given in table 1. The efficiency changes depending on the plasma density, so it is required to carefully choose the plasma density for the second PWFA stage in order to increase the energy transfer efficiency. For a very high plasma density, the driving bunch can become too long compared with the plasma wavelength (determined by the dimensionless value $k_p\xi_b$ in table 1), leading to its tail being accelerated in the created bubble and a significant drop in the driver-to-plasma energy transfer efficiency due to non-uniformity of the field distribution. The efficiency can, thus, be increased by lowering the plasma density. In very low-density plasmas, the efficiency also starts to slightly drop due to the non-uniformity of the field at the front of a short driver. In addition, lower

https://doi.org/10.1017/S0022377823001162 Published online by Cambridge University Press

densities can be less desirable due to lower acceleration gradients, which increase the size of the accelerator. Therefore, there is an optimal range of plasma densities at which the beam-to-plasma efficiency is high. As results of numerical simulations show (table 1), for the considered electron driver, the optimal plasma density of the second PWFA stage is around $10^{18}\,\mathrm{cm}^{-3}$, corresponding to the length of the driver in plasma units $k_p\xi_b \sim 3$.

3. Downramp injection

In this section, we study the dependence of the current profile of the witness electron beam produced by density-downramp injection on the driver and plasma parameters. A recent study on downramp injection for LWFA (Hue *et al.* 2023) reports that the injected beam current is strongly influenced by the laser intensity and, consecutively, the wakefield strength. Unlike for the laser driven counterpart, the electron driver can be considered non-evolving during the beam injection process in the PWFA stage since the beam evolution scale is the period of betatron oscillations $\sqrt{2\gamma}\lambda_p$, usually of millimetre to centimetre scale, much longer than the downramp length, usually in the range of hundreds of micrometres or less. As a result, the location of the downramp does not play such a crucial role as in the LWFA case.

3.1. *The influence of downramp steepness*

Now we consider the influence of downramp steepness on the parameters of the injected beam. As quasistatic codes such as QuickPIC used in § 2 cannot self-consistently describe the injection of particles into the wakefield, we perform PIC simulations with FBPIC (Lehe *et al.* 2016) which is a spectral quasi-3-D PIC code with angular mode decomposition. In the simulations, we use a simulation box of the 80 µm size with 2048 cells in the longitudinal z direction and the 50 µm size with 640 cells in the radial r direction. The number of the angular modes is equal to 2, and the total number of particles per cell is 45 (5 in the angular direction and 3×3 in the zr plane). The timestep is equal to the longitudinal grid cell size, $\Delta t = \Delta z/c$, and simulations are performed in a moving window with the velocity of c.

The downramp is modelled as a linear change of plasma density from n_0 to $n_0/2$ of length L. For a given downramp steepness, particles are injected only when their energy is high enough, the required energy grows with the decrease of the downramp steepness (Xu *et al.* 2017). The energy of the particles depends only on the nonlinearity of the created bubble (which will be quantified later) irrespective of other driver properties.

Four group of simulations are presented in figure 2 that explain the role that the nonlinearity of the bubble (which depends on the density ratio n_b/n_0 between the driver and the plasma for a fixed driver shape and size) and L play on the witness injection. The injected beam currents are plotted and the corresponding wakefield structures are illustrated in the insets of figure 2(*c*,*g*). As figure 2(*b*) demonstrates, for a fixed downramp length L, the injection occurs only when the bubble nonlinearity is strong enough. In addition, once the condition for injection is reached, the witness beam current is barely influenced by the downramp steepness for the same bubble strength (the same driver), as shown in figure 2(*c*). Similar to the results in Ekerfelt *et al.* (2017), Silva *et al.* (2019) and Hue *et al.* (2023), a current peak is observed at the head of the witness bunch. This happens due to the nonlinear phase mixing caused by a sharp plasma density transition when the downramp begins, and the peak can be mitigated with a smooth density transition at the beginning of the downramp, usually found in experimental cases. Behind the head of the bunch with respect to the comoving coordinate $\xi = z - ct$, the injected current stabilises at a constant value. Therefore, in the following considerations, we define the value of the injected witness current J_w as the average current (independent of coordinate

https://doi.org/10.1017/S0022377823001162 Published online by Cambridge University Press

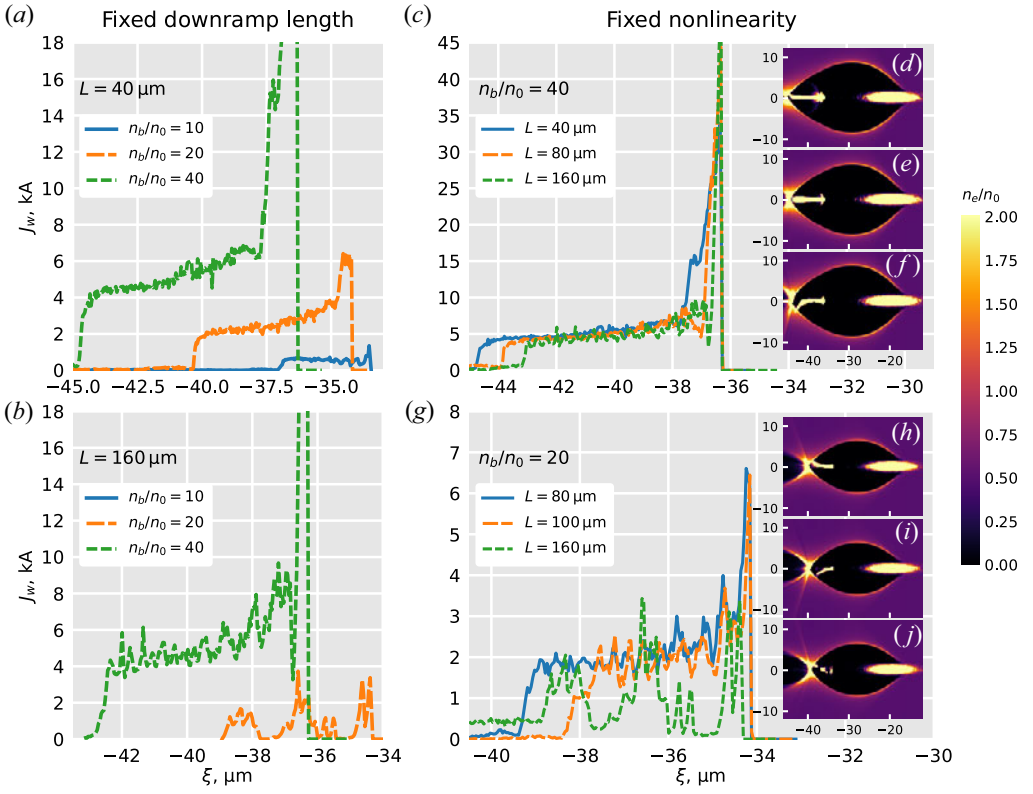

FIGURE 2. Current profiles of injected beam J_w corresponding to different lengths of plasma density downramp L and different wakefield nonlinearity n_b/n_0. The insets are wakefield structures for the plotted simulations. Plasma density before the downramp $n_0 = 5 \times 10^{18}\,\mathrm{cm}^{-3}$; $n_0/2$ after the downramp. The driver has the Gaussian shape with $\sigma_z = 2.5\,\mu\mathrm{m}$ and $\sigma_r = 0.5\,\mu\mathrm{m}$.

ξ) of the constant part of the profile. As figure 2(*c*,*g*) and corresponding insets show, the length and thus the charge of the injected beam get slightly smaller with the increase in the transition length L (in particular, in figure 2(*c*), the charges of the injected bunches are 209, 175 and 148 pC, whereas in figure 2(*g*) the charges are 39, 28 and 21 pC). However, it is still mostly determined by the ratio between the initial and the final plasma density (fixed at 2 in our case), as this ratio determines the increase in the length of the bubble during the transition. The value of the injected beam current J_w is even less dependent on the transition length (except the green line in figure 2(*g*) where the downramp length is already close to the injection threshold and injection does not result in a flat current profile).

As shown by figure 2(*a*,*b*), the higher value of ratio n_b/n_0 (and, thus, the wakefield nonlinearity) leads to the higher current J_w. From the comparison of figures 2(*a*) and 2(*b*), one can see that shorter and steeper downramp enables injection at lower driver charge and lower nonlinearity. No injection at all is observed for the case where $n_b/n_0 = 10$ shown in (*b*), and the higher the wakefield nonlinearity n_b/n_0 is, the stronger the injected witness current becomes.

3.2. *Injected beam current scaling*

As shown in the previous section, as long as the density downramp provides stable injection, its properties do not significantly affect the injected current J_w (defined now

https://doi.org/10.1017/S0022377823001162 Published online by Cambridge University Press

as the average value of the constant part of the injected bunch current profile), so it should mostly be determined by the parameters of the driver and their relation to the plasma density. It is suggested by figure 2 that the higher values of n_b/n_0 which should correspond to stronger nonlinearity lead to a stronger injected beam current. As we want to investigate the dependence of J_w on the nonlinearity of the bubble, we need to introduce a measure of it first. In the previous section, we used the ratio n_b/n_0 as this measure, which is only suitable for a fixed shape and size of the driver. A more general measure requires introducing the energy properties of the bubble.

Following Lotov (2004) and Golovanov *et al.* (2021, 2023), we introduce the quantity $\Psi(\xi) = \int (cW - S_z)\,\mathrm{d}^2 r_\perp$ which depends on the comoving coordinate $\xi = z - ct$ and contains the integral over the transverse plane of the energy density W and the longitudinal energy flux S_z of both the electromagnetic field and the plasma particles. The value of Ψ is also equal to the total energy flux in the comoving window (Lotov 2004). As it has the dimension of power, we will refer to Ψ as 'the power of the bubble'. In the absence of energy exchange with bunches, Ψ is a conserved property in any wake; drivers lead to the increase of Ψ, whereas accelerated witnesses decrease it. As a property describing the energetic properties of the bubble, it is equal to the total power of deceleration felt by the driving bunch and is also equal to the maximum achievable power of acceleration for the witness bunch. For the blowout regime of plasma wakefield, Ψ is fully determined by the size of the bubble R_{bub} and grows with it; in the limit of a large bubble size ($k_p R_{\mathrm{bub}} \gg 1$), $\Psi \propto (k_p R_{\mathrm{bub}})^4$ (see Tzoufras *et al.* 2008; Golovanov *et al.* 2021). The power of the bubble Ψ serves as quantification of nonlinearity of the wake and it is the most important property of the bubble. Regardless of the shape the driver which creates a bubble with a certain value of Ψ, the effect of the bubbles with the same power on acceleration of particles and on downramp injection will be mostly the same. Therefore, we can expect that injection only depends on the value of Ψ.

According to Golovanov *et al.* (2021), for a blowout wakefield excited by a sufficiently tightly focused ($k_p r_b \ll 1$) driver with the charge Q and a flattop current profile of length ξ_b, the power of the bubble in the large-bubble limit ($k_p R_{\mathrm{bub}} \gg 1$) is calculated using the following formula:

$$\Psi \approx \frac{4\pi m^2 c^6 \varepsilon_0}{e^2 J_A} k_p Q \left[\sqrt{\frac{2cQ}{J_A \xi_b}} - \frac{k_p \xi_b}{8}\right], \tag{3.1}$$

where $J_A = 4\pi\varepsilon_0 mc^3/e \approx 17\,\mathrm{kA}$ is the Alfvén current. It can be rewritten as

$$\Psi \approx \frac{\sqrt{2} mc^2 J_A}{e} \left(\frac{J_{\mathrm{eff}}}{J_A}\right)^{3/2} \left[1 - \frac{(k_p \xi_b)^{4/3}}{\sqrt{128 J_{\mathrm{eff}}/J_A}}\right], \tag{3.2}$$

where we introduce the quantity J_{eff} which we call 'the effective current' of the driver:

$$J_{\mathrm{eff}} = \frac{cQ}{\xi_b} (k_p \xi_b)^{2/3} = J_b (k_p \xi_b)^{2/3}. \tag{3.3}$$

For high-current ($J_{\mathrm{eff}} \sim J_A$) sufficiently short electron bunches, the last factor in (3.2) is close to 1, and $\Psi \propto J_{\mathrm{eff}}^{3/2}$. In general, this factor describes the weakening of the bubble when the bunch becomes long enough compared with the plasma wavelength. In the limiting case when the back of the bunch is already located in the accelerating phase, the bubble effectively transfers the energy from one part of the driver to another, limiting the possible efficiency of accelerating the witness, which corresponds to this factor tending

https://doi.org/10.1017/S0022377823001162 Published online by Cambridge University Press

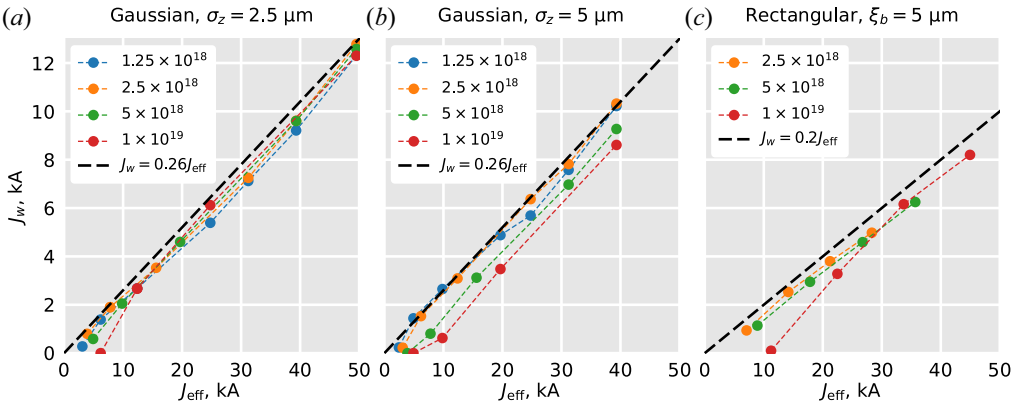

FIGURE 3. The relationship between J_w and J_{eff} for different types of beams. Each line corresponds to the same value of plasma density (in cm^{-3} in the legend), and the driver beam current J_b is varied while the beam longitudinal size (σ_z or ξ_b) remains the same. The dashed black line corresponds to the linear dependence on J_w.

to 0. When it becomes negative, this solution for Ψ is formally incorrect, which corresponds to the situation when the driver cannot fit inside the bubble.

Since J_{eff} fully determines Ψ and, thus, the properties of the bubble for sufficiently short bunches, it should be the only combination of the driver and plasma parameters affecting the injection process. Although the model in Golovanov *et al.* (2021) is not necessarily strictly valid in the case of smaller-size bubbles, because this dependence holds in the important limit of large bubbles, we make a conjecture that J_{eff} should be the most important combination of the driver's parameters.

To explore the influence of J_{eff} on the injected witness current J_w, we perform numerical PIC simulations with FBPIC (Lehe *et al.* 2016) for two types of drivers: 3-D Gaussian beams which are usually used to model the driver beam produced by a conventional accelerator (Joshi *et al.* 2018; D'Arcy *et al.* 2019), and flattop longitudinal bunch which models the LWFA produced driver beam (Couperus Cabadağ *et al.* 2021; Foerster *et al.* 2022). To prevent any effects due to the evolution of the driver beam, we artificially freeze it by setting its initial particle energy to 50 GeV. The ratio between the plasma density before and after the downramp is fixed to 2 (going from n_0 to $n_0/2$) and the downramp length is between 20 μm and 160 μm. For Gaussian drivers with the density profile defined as $n_b \exp[-r^2/2\sigma_r^2 - (\xi - \xi_0)^2/2\sigma_z^2]$, the beam transverse size $\sigma_r = 0.5$ μm. Flattop drivers correspond to the cylinder of constant density n_b, length ξ_b and fixed radius $r_b = 0.6$ μm.

As the effective current J_{eff} defined by (3.3) depends on the current of the driver J_b and its length ξ_b, we study the relationship J_w and J_{eff} by varying these two parameters. Of course, the value of J_{eff} also depends on the plasma density, so we use the plasma density n_0 before the downramp to calculate the plasma wavenumber k_p used in (3.3). Because definition (3.3) is written for flattop profiles, for Gaussian beams we use $\xi_b = \sqrt{2}\sigma_z$ and the peak value of J_b. This combination was shown to provide a good approximation for Ψ in simulations (not presented in the paper). The results for varying the driver beam current J_b at fixed length are shown in figure 3, and the results for varying the driver bunch length while the current is fixed are presented in figure 4 for different plasma densities.

For the fixed beam length (figure 3), we observe a linear dependence of the injected current on the effective current, which seems to indicate that $J_w \propto \Psi^{2/3} \propto J_{\text{eff}}$. The slope

https://doi.org/10.1017/S0022377823001162 Published online by Cambridge University Press

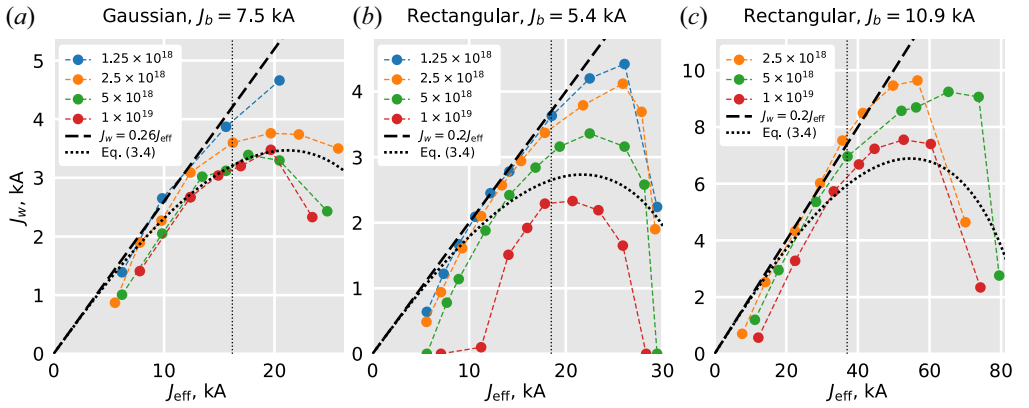

FIGURE 4. The relationship between J_w and J_{eff} for different types of beams and different beam currents. Each dashed line corresponds to the same value of plasma density (in cm^{-3} in the legend), and the driver beam longitudinal size ξ_b is varied while the driver current J_b remains the same. The dashed black line corresponds to the linear dependence on J_w. The dotted line shows the prediction according to (3.4) with a correction $c_2 = 0.8$ for the Gaussian shape and 0.4 for the rectangular shape. The vertical lines correspond to the J_{eff} value above which the length of the driver becomes comparable to the plasma wavelength ($\sigma_z = \lambda_p/2\sqrt{2}$ for the Gaussian shape and $\xi_b = \lambda_p$ for the rectangular shape).

of the linear dependence depends only on the shape of the driver and remains the same for different plasma densities and lengths of the driver. We observe that the witness current becomes slightly lower for denser plasmas (thus, larger values of k_p), which corresponds to the lowering efficiency due to the driver length in plasma units, as predicted by the length factor in (3.2). At very low J_{eff}, the injected current goes to 0, which corresponds to the injection threshold discussed in § 3.1.

To study the dependence of the witness current J_w on the driver length ξ_b in more details, we also plot the dependence of J_w on the effective current J_{eff} for a fixed current of the driver, which means that the increase in J_{eff} corresponds to the increase in its length (figure 4). For smaller J_{eff} and, thus, shorter driver lengths, the already found linear trend with the same slope is again observed for both types of drivers. But for higher J_{eff} and longer driver length, we see the deviation of J_w from the linear trend and the decline in it. This behaviour is qualitatively consistent with (3.2) which predicts that the elongation of the driver lowers the efficiency of exciting a bubble, so we can expect that the witness current $J_w \propto \Psi^{2/3}$ behaves as

$$J_w = c_1 J_{\text{eff}} \left[1 - c_2 \frac{(k_p \xi_b)^{4/3}}{\sqrt{128 J_{\text{eff}}/J_A}}\right]^{2/3}. \tag{3.4}$$

By choosing the value of c_2, the qualitative behaviour of J_{eff} can be recreated using this formula (see the dotted lines in figure 4).

However, this formula cannot show the full picture, because downramp injection for longer drivers is more complex than for short drivers. According to (3.2), the power of the bubble changes as the driver propagates through the density downramp which changes the plasma wavenumber k_p. For short drivers, $\Psi \propto J_{\text{eff}}^{3/2} \propto n_p^{1/2}$ scales exactly the same for all drivers with the same J_{eff} and, thus, the injected current is still fully determined by J_{eff}. However, longer drivers which have a lowered efficiency in dense plasma begin

https://doi.org/10.1017/S0022377823001162 Published online by Cambridge University Press

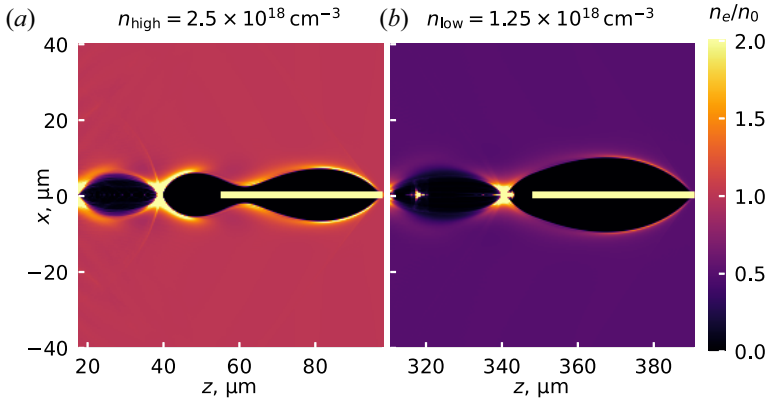

FIGURE 5. Electron density distribution in a wake excited by a long rectangular-shape driver before and after the downramp. The downramp provides transition from n_0 to $n_0/2$ where $n_0 = 2.5 \times 10^{18}\,\mathrm{cm}^{-3}$. The parameters of the driver: $n_b = 40n_0$, $\xi_b = 42.5\,\mu\mathrm{m}$ and $r_b = 0.6\,\mu\mathrm{m}$.

exciting the bubble more effectively when transitioning into lower-density plasma at the downramp, as their length in plasma units becomes small. An example of such a driver is shown in figure 5: in the initial higher density it is too long to fit inside the bubble, so during the density downramp it passes through the point of having almost zero efficiency of exciting a bubble ($\Psi \approx 0$), and then Ψ starts growing again as the driver becomes shorter than the excited bubble. In addition to the complex behaviour of the nonlinearity of the bubble, the corresponding velocity of the back of the bubble which determines the injection threshold will also significantly depend on the length of the driver. The dynamics of downramp injection for such cases cannot be reduced to a simple formula such as linear dependence on J_{eff} or even corrected (3.4) and requires the full description of the evolution of the bubble in the downramp. However, as explained in § 2, these cases are suboptimal for efficient utilisation of the driver's energy and should be avoided. In more optimal cases, when the driver is comparatively short, the linear dependence of J_w and J_{eff} holds.

4. Conclusion

We have studied a PWFA driven by a short high-current electron bunch. The accelerating structure in this case remains stable until the moment when some of the electrons of the driver lose all their energy, which is the condition which determines the acceleration length optimising the driver-to-plasma energy transfer efficiency. The dependence of the witness bunch generated by density-downramp injection on the parameters of the driver has been studied. We have shown that a steeper downramp enables injection for a weaker driver, but the current of the injected bunch does not significantly depend on the downramp length as long as the criterion for the injection is met. The witness current of the injected bunch mostly depends on the effective current of the driver J_{eff} which combines both the driver's current and its length in plasma units. The dependence of the injected witness current on the effective current is linear for reasonably short drivers.

Acknowledgements

Editor Luís O. Silva thanks the referees for their advice in evaluating this article.

https://doi.org/10.1017/S0022377823001162 Published online by Cambridge University Press

Funding

This work was supported by the Fondation Jacques Toledano, the Schwartz Reisman Center for Intense Laser Physics, and by EIC ebeam4therapy grant.

Declaration of interests

The authors report no conflict of interest.

Data availability statement

The simulation data are available on request from the corresponding author, A.G.

REFERENCES

AN, W., ZHOU, M., VAFAEI-NAJAFABADI, N., MARSH, K.A., CLAYTON, C.E., JOSHI, C., MORI, W.B., LU, W., ADLI, E., CORDE, S., *et al.* 2013 Strategies for mitigating the ionization-induced beam head erosion problem in an electron-beam-driven plasma wakefield accelerator. *Phys. Rev. ST Accel. Beams* **16** (10), 101301.

BLUMENFELD, I., CLAYTON, C.E., DECKER, F.-J., HOGAN, M.J., HUANG, C., ISCHEBECK, R., IVERSON, R., JOSHI, C., KATSOULEAS, T., KIRBY, N., *et al.* 2007 Energy doubling of 42 GeV electrons in a metre-scale plasma wakefield accelerator. *Nature* **445** (7129), 741–744.

BLUMENFELD, I., CLAYTON, C.E., DECKER, F.J., HOGAN, M.J., HUANG, C., ISCHEBECK, R., IVERSON, R.H., JOSHI, C., KATSOULEAS, T., KIRBY, N., *et al.* 2010 Scaling of the longitudinal electric field and transformer ratio in a nonlinear plasma wakefield accelerator. *Phys. Rev. ST Accel. Beams* **13**, 111301.

CHEN, P., DAWSON, J.M., HUFF, R.W. & KATSOULEAS, T. 1985 Acceleration of electrons by the interaction of a bunched electron beam with a plasma. *Phys. Rev. Lett*. **54**, 693–696.

COUPERUS CABADAĞ, J.P., PAUSCH, R., SCHÖBEL, S., BUSSMANN, M., CHANG, Y.-Y., CORDE, S., DEBUS, A., DING, H., DÖPP, A., FOERSTER, F.M., *et al.* 2021 Gas-dynamic density downramp injection in a beam-driven plasma wakefield accelerator. *Phys. Rev. Res*. **3**, L042005.

D'ARCY, R., ASCHIKHIN, A., BOHLEN, S., BOYLE, G., BRÜMMER, T., CHAPPELL, J., DIEDERICHS, S., FOSTER, B., GARLAND, M.J., GOLDBERG, L., *et al.* 2019 FLASHForward: plasma wakefield accelerator science for high-average-power applications. *Phil. Trans. R. Soc.* A **377** (2151), 20180392.

EKERFELT, H., HANSSON, M., GONZÁLEZ, I.G., DAVOINE, X. & LUNDH, O. 2017 A tunable electron beam source using trapping of electrons in a density down-ramp in laser wakefield acceleration. *Sci. Rep*. **7** (1), 12229.

ESAREY, E., SCHROEDER, C.B. & LEEMANS, W.P. 2009 Physics of laser-driven plasma-based electron accelerators. *Rev. Mod. Phys*. **81** (3), 1229–1285.

FAURE, J., RECHATIN, C., NORLIN, A., LIFSCHITZ, A., GLINEC, Y. & MALKA, V. 2006 Controlled injection and acceleration of electrons in plasma wakefields by colliding laser pulses. *Nature* **444** (7120), 737–739.

FOERSTER, F.M., DÖPP, A., HABERSTROH, F., GRAFENSTEIN, K.V., CAMPBELL, D., CHANG, Y.-Y., CORDE, S., COUPERUS CABADAĞ, J.P., DEBUS, A., GILLJOHANN, M.F., *et al.* 2022 Stable and high-quality electron beams from staged laser and plasma wakefield accelerators. *Phys. Rev.* X **12**, 041016.

GOLOVANOV, A.A., KOSTYUKOV, I.YU., REICHWEIN, L., THOMAS, J. & PUKHOV, A. 2021 Excitation of strongly nonlinear plasma wakefield by electron bunches. *Plasma Phys. Control. Fusion* **63** (8), 085004.

GOLOVANOV, A., KOSTYUKOV, I.YU., PUKHOV, A. & MALKA, V. 2023 Energy-conserving theory of the blowout regime of plasma wakefield. *Phys. Rev. Lett*. **130** (10), 105001.

GONSALVES, A.J., NAKAMURA, K., DANIELS, J., BENEDETTI, C., PIERONEK, C., DE RAADT, T.C.H., STEINKE, S., BIN, J.H., BULANOV, S.S., VAN TILBORG, J., *et al.* 2019 Petawatt laser guiding and electron beam acceleration to 8 GeV in a laser-heated capillary discharge waveguide. *Phys. Rev. Lett*. **122**, 084801.

GREBENYUK, J., MARTINEZ DE LA OSSA, A., MEHRLING, T. & OSTERHOFF, J. 2014 Beam-driven plasma-based acceleration of electrons with density down-ramp injection at flashforward. *Nucl. Instrum. Meth. Phys. Res.* A **740**, 246–249.

HIDDING, B., KÖNIGSTEIN, T., OSTERHOLZ, J., KARSCH, S., WILLI, O. & PRETZLER, G. 2010 Monoenergetic energy doubling in a hybrid laser-plasma wakefield accelerator. *Phys. Rev. Lett*. **104** (19), 195002.

HUANG, C., DECYK, V.K., REN, C., ZHOU, M., LU, W., MORI, W.B., COOLEY, J.H., ANTONSEN, T.M. JR. & KATSOULEAS, T. 2006 QUICKPIC: a highly efficient particle-in-cell code for modeling wakefield acceleration in plasmas. *J. Comput. Phys*. **217** (2), 658–679.

HUANG, C., LU, W., ZHOU, M., CLAYTON, C.E., JOSHI, C., MORI, W.B., MUGGLI, P., DENG, S., OZ, E., KATSOULEAS, T., *et al.* 2007 Hosing instability in the blow-out regime for plasma-wakefield acceleration. *Phys. Rev. Lett*. **99**, 255001.

HUE, C.S., WAN, Y., LEVINE, E.Y. & MALKA, V. 2023 Control of electron beam current, charge, and energy spread using density downramp injection in laser wakefield accelerators. *Matter Radiat. Extremes* **8** (2), 024401.

JOSHI, C., ADLI, E., AN, W., CLAYTON, C.E., CORDE, S., GESSNER, S., HOGAN, M.J., LITOS, M., LU, W., MARSH, K.A., *et al.* 2018 Plasma wakefield acceleration experiments at Facet II. *Plasma Phys. Control. Fusion* **60** (3), 034001.

KURZ, T., HEINEMANN, T., GILLJOHANN, M.F., CHANG, Y.Y., COUPERUS CABADAĞ, J.P., DEBUS, A., KONONENKO, O., PAUSCH, R., SCHÖBEL, S., ASSMANN, R.W., *et al.* 2021 Demonstration of a compact plasma accelerator powered by laser-accelerated electron beams. *Nat. Commun*. **12** (1), 2895.

LEHE, R., KIRCHEN, M., ANDRIYASH, I.A., GODFREY, B.B. & VAY, J.-L. 2016 A spectral, quasi-cylindrical and dispersion-free particle-in-cell algorithm. *Comput. Phys. Commun*. **203**, 66–82.

LI, S.Z., ADLI, E., ENGLAND, R.J., FREDERICO, J., GESSNER, S.J., HOGAN, M.J., LITOS, M.D., WALZ, D.R., MUGGLI, P., AN, W., *et al.* 2012 Head erosion with emittance growth in PWFA. *AIP Conf. Proc*. **1507** (1), 582–587.

LINDSTRØM, C.A., GARLAND, J.M., SCHRÖDER, S., BOULTON, L., BOYLE, G., CHAPPELL, J., D'ARCY, R., GONZALEZ, P., KNETSCH, A., LIBOV, V., *et al.* 2021 Energy-spread preservation and high efficiency in a plasma-wakefield accelerator. *Phys. Rev. Lett*. **126** (1), 014801.

LITOS, M., ADLI, E., AN, W., CLARKE, C.I., CLAYTON, C.E., CORDE, S., DELAHAYE, J.P., ENGLAND, R.J., FISHER, A.S., FREDERICO, J., *et al.* 2014 High-efficiency acceleration of an electron beam in a plasma wakefield accelerator. *Nature* **515** (7525), 92–95.

LOTOV, K.V. 2004 Blowout regimes of plasma wakefield acceleration. *Phys. Rev.* E **69**, 046405.

LU, W., HUANG, C., ZHOU, M., MORI, W.B. & KATSOULEAS, T. 2006 Nonlinear theory for relativistic plasma wakefields in the blowout regime. *Phys. Rev. Lett*. **96**, 165002.

MALKA, V., FAURE, J., GAUDUEL, Y.A., LEFEBVRE, E., ROUSSE, A. & PHUOC, K.T. 2008 Principles and applications of compact laser–plasma accelerators. *Nat. Phys*. **4** (6), 447–453.

MARTINEZ DE LA OSSA, A., HU, Z., STREETER, M.J.V., MEHRLING, T.J., KONONENKO, O., SHEERAN, B. & OSTERHOFF, J. 2017 Optimizing density down-ramp injection for beam-driven plasma wakefield accelerators. *Phys. Rev. Accel. Beams* **20**, 091301.

MEHRLING, T.J., FONSECA, R.A., DE LA OSSA, A.M. & VIEIRA, J. 2017 Mitigation of the hose instability in plasma-wakefield accelerators. *Phys. Rev. Lett*. **118** (17), 174801.

MEHRLING, T.J., FONSECA, R.A., MARTINEZ DE LA OSSA, A. & VIEIRA, J. 2019 Mechanisms for the mitigation of the hose instability in plasma-wakefield accelerators. *Phys. Rev. Accel. Beams* **22** (3), 031302.

MUGGLI, P., BLUMENFELD, I., CLAYTON, C.E., DECKER, F.J., HOGAN, M.J., HUANG, C., ISCHEBECK, R., IVERSON, R.H., JOSHI, C., KATSOULEAS, T., *et al.* 2010 Energy gain scaling with plasma length and density in the plasma wakefield accelerator. *New J. Phys*. **12** (4), 045022.

PUKHOV, A. & MEYER-TER-VEHN, J. 2002 Laser wake field acceleration: the highly non-linear broken-wave regime. *Appl. Phys.* B **74** (4–5), 355–361.

ROSENZWEIG, J.B., BREIZMAN, B., KATSOULEAS, T. & SU, J.J. 1991 Acceleration and focusing of electrons in two-dimensional nonlinear plasma wake fields. *Phys. Rev.* A **44** (10), R6189–R6192.

Silva, T., Helm, A., Vieira, J., Fonseca, R. & Silva, L.O. 2019 On the use of the envelope model for down-ramp injection in laser-plasma accelerators. *Plasma Phys. Control. Fusion* **62** (2), 024001.

Tajima, T. & Dawson, J.M. 1979 Laser electron accelerator. *Phys. Rev. Lett*. **43**, 267–270.

Tzoufras, M., Lu, W., Tsung, F.S., Huang, C., Mori, W.B., Katsouleas, T., Vieira, J., Fonseca, R.A. & Silva, L.O. 2008 Beam loading in the nonlinear regime of plasma-based acceleration. *Phys. Rev. Lett*. **101**, 145002.

Xu, X.L., Li, F., An, W., Dalichaouch, T.N., Yu, P., Lu, W., Joshi, C. & Mori, W.B. 2017 High quality electron bunch generation using a longitudinal density-tailored plasma-based accelerator in the three-dimensional blowout regime. *Phys. Rev. Accel. Beams* **20**, 111303.

Zhang, C., Huang, C.-K., Marsh, K.A., Xu, X.L., Li, F., Hogan, M., Yakimenko, V., Corde, S., Mori, W.B. & Joshi, C. 2019 Effect of fluctuations in the down ramp plasma source profile on the emittance and current profile of the self-injected beam in a plasma wakefield accelerator. *Phys. Rev. Accel. Beams* **22** (11), 111301.

Zhou, M., Clayton, C.E., Huang, C., Joshi, C., Lu, W., Marsh, K.A., Mori, W.B., Katsouleas, T., Muggli, P., Oz, E., *et al.* 2007 Beam head erosion in self-ionized plasma wakefield accelerators. In *2007 IEEE Particle Accelerator Conference*. IEEE, pp. 3064–3066.

https://doi.org/10.1017/S0022377823001162 Published online by Cambridge University Press